International Journal of Biochemistry and Cell Biology 97 (2018) 52–61

Contents lists available at ScienceDirect

International Journal of Biochemistry and Cell Biology

journal homepage: www.elsevier.com/locate/biocel

# Identification of a high affinity binding site for abscisic acid on human lanthionine synthetase component C-like protein 2

Elena Cichero[a,1], Chiara Fresia[b,1], Lucrezia Guida[b], Valeria Booz[b], Enrico Millo[b,c], Claudia Scotti[d,e], Luisa Iamele[d,e], Hugo de Jonge[d,e], Denise Galante[f], Antonio De Flora[b], Laura Sturla[b,c,*], Tiziana Vigliarolo[b,*], Elena Zocchi[b,c], Paola Fossa[a,*]

[a] Department of Pharmacy, Section of Medicinal Chemistry, School of Medical and Pharmaceutical Sciences, University of Genoa, Viale Benedetto XV 3, 16132, Genoa, Italy
[b] Department of Experimental Medicine, Section of Biochemistry, School of Medical and Pharmaceutical Sciences, University of Genoa, Viale Benedetto XV 1, 16132, Genoa, Italy
[c] Center of Excellence for Biomedical Research (CEBR), University of Genoa, Via G.B. Marsano 10, 16132, Genoa, Italy
[d] Department of Molecular Medicine, Immunology and General Pathology Unit, University of Pavia, Via Ferrata 9, 27100, Pavia, Italy
[e] Ardis Srl, Via Taramelli 24, 27100, Pavia, Italy
[f] Institute for Macromolecular Studies, National Research Council, Genova, Italy

ARTICLE INFO

*Keywords:*
Human lanthionine synthetase component C-like protein 2 (LANCL2)
Abscisic acid (ABA)
Binding affinity
Computational studies
Site-directed mutagenesis

ABSTRACT

Lanthionine synthetase component C-like protein 2 (LANCL2) has been identified as the mammalian receptor mediating the functional effects of the universal stress hormone abscisic acid (ABA) in mammals. ABA stimulates insulin independent glucose uptake in myocytes and adipocytes via LANCL2 binding *in vitro*, improves glucose tolerance *in vivo* and induces brown fat activity *in vitro* and *in vivo*. The emerging role of the ABA/LANCL2 system in glucose and lipid metabolism makes it an attractive target for pharmacological interventions in diabetes mellitus and the metabolic syndrome. The aim of this study was to investigate the presence of ABA binding site (s) on LANCL2 and identify the amino acid residues involved in ABA binding. Equilibrium binding assays ([$^3$H]-ABA saturation binding and surface plasmon resonance analysis) suggested multiple ABA-binding sites, prompting us to perform a computational study that indicated one putative high-affinity and two low-affinity binding sites. Site-directed mutagenesis (single mutant R118I, triple mutants R118I/R22I/K362I and R118I/S41A/E46I) and equilibrium binding experiments on the mutated LANCL2 proteins identified a high-affinity ABA-binding site involving R118, with a $K_D$ of 2.6 nM ± 1.2 nM, as determined by surface plasmon resonance. Scatchard plot analysis of binding curves from both types of equilibrium binding assays revealed a Hill coefficient > 1, suggesting cooperativity of ABA binding to LANCL2. Identification of the high-affinity ABA-binding site is expected to allow the design of ABA agonists/antagonists, which will help to understand the role of the ABA/LANCL2 system in human physiology and disease.

## 1. Introduction

The lanthionine synthetase C-like (LANCL) enzyme family comprises the eukaryotic homologues of the prokaryotic lanthionine synthetase component C (LanC) protein, a zinc-containing enzyme involved in the modification of peptides and lanthionines (Bauer et al., 2000).

LANCL1 was the first member of this family to be isolated from human erythrocyte membranes (Mayer et al., 1998). LANCL2 was subsequently identified in the central nervous system, as well as in immune cells, heart, placenta, lung, liver, pancreas, prostate and skeletal muscles (Mayer et al., 2001). The two proteins share a significant sequence homology (> 70%) but differ in their subcellular localization: LANCL1 is cytosolic, while LANCL2 is bound to the plasma membrane through its myristoylated N-terminal Gly residue (Landlinger et al., 2006; Fresia et al., 2016). A third member of the LANCL protein family, LANCL3, is expressed at very low levels in human cells (Sturla et al., 2009). Despite the name “lanthionine synthetase”, none of the LANCL

*Abbreviations:* LANCL2, human lanthionine synthetase component C-like protein 2; ABA, abscisic acid; SPR, surface plasmon resonance; GST, glutathione *S*-transferase; cADPR, cyclic adenosine diphosphate-ribose; PKA, protein kinase A; DTT, dithiothreitol

* Corresponding authors.
*E-mail addresses:* laurasturla@unige.it (L. Sturla), tiziana.vigliarolo@edu.unige.it (T. Vigliarolo), fossa@difar.unige.it (P. Fossa).
[1] These authors equally contributed to this work.

https://doi.org/10.1016/j.biocel.2018.02.003
Received 12 June 2017; Received in revised form 25 January 2018; Accepted 2 February 2018
Available online 05 February 2018
1357-2725/ 

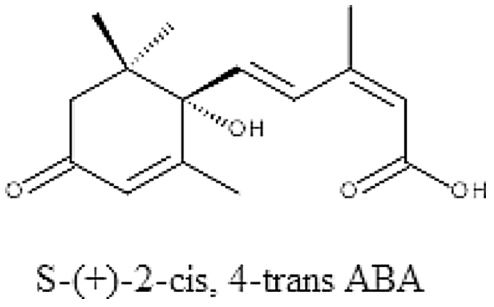


**Fig. 1.** Chemical structure of S-(+)-2-cis, 4-trans abscisic acid (ABA).

proteins is involved in lanthionine synthesis in mammals (He et al., 2017).

Recently, *in vitro* and *in vivo* studies performed on purified human recombinant LANCL2 and on the protein overexpressed in animal cells demonstrated that LANCL2 binds 2-cis, 4-trans abscisic acid (ABA) (Sturla et al., 2009, 2011). ABA is an isoprenoid hormone (Fig. 1) regulating seed dormancy and germination and the plant response to environmental stress, such as changes in water, light and nutrient availability (Nambara and Marion-Poll, 2005). ABA has a chiral center in its molecule, yielding the enantiomers (R)-(−) ABA and (S)-(+) ABA; many reports demonstrate that both enantiomers show hormonal activitiy in many assay systems in plants (Lin et al., 2005).

With a fundamentally conserved role as a stress hormone, ABA is also present and active in animals (Lievens et al., 2017), where it induces the activation of innate immune cells (the first line of defense against biotic and abiotic cues) (Bruzzone et al., 2007; Magnone et al., 2009), and plays a role in the regulation of glycemia. Glucose intake induces an increase of plasma ABA in healthy humans (Bruzzone et al., 2012) and ABA stimulates insulin release from pancreatic beta cells and glucose uptake by muscle and adipose cells *in vitro* (Bruzzone et al., 2008, 2012). In mammals both R-(−) and S-(+) enantiomers are biologically active on granulocytes (Bruzzone et al., 2007) and on insulin-releasing cells (Bruzzone et al., 2008). Intake of ABA reduces glycemia after a glucose load both in rodents and in humans (Magnone et al., 2015). Interestingly, the reduced blood glucose area under curve after a carbohydrate load is not due to an increased insulinemia: on the contrary, plasma insulin is lower in ABA-treated vs. untreated animals, suggesting that *in vivo* the effect of ABA on tissue glucose uptake may prevail over its insulin-releasing action (Magnone et al., 2015).

The functional effects of ABA on innate immune and on beta-cells are mediated by LANCL2, as demonstrated by the amplification or inhibition of the response to ABA in target cells transfected with a LANCL2-encoding plasmid or with a LANCL2-specific siRNA, respectively (Sturla et al., 2009). The signaling pathway downstream of ABA binding to membrane-bound LANCL2 involves the sequential activation of a G protein, the cAMP-dependent activation of PKA and CD38 phosphorylation, leading to a cyclic ADP-ribose (cADPR)-mediated intracellular $Ca^{2+}$ increase (Bruzzone et al., 2007, 2008; Magnone et al., 2009; Bodrato et al., 2009). Mutation of N-terminal Glycine (Gly2) prevents myristoylation of LANCL2 and abrogates the ABA-triggered signaling via cAMP (Fresia et al., 2016). Interestingly, ABA binding also induces the nuclear translocation of LANCL2 in transfected cells, making human LANCL2 an unprecedented example of a non-transmembrane G protein-coupled receptor also capable of hormone-induced nuclear translocation (Fresia et al., 2016). In addition to activation of PKA, ABA also induces activation of Akt. An increased phosphorylation level on Ser-473 of Akt was observed in adipocytes and myocytes incubated with ABA (Bruzzone et al., 2012). Indeed, Zeng et al. (2014) have demonstrated that LANCL2 is a positive regulator of Akt activation in human liver cells by enhancing Akt phosphorylation at Ser-473by mTORC2.

The apparent $K_D$ of human recombinant LANCL2 for ABA, as calculated from equilibrium binding experiments on the purified protein, was reported to be in the high micromolar range (Sturla et al., 2011) consistent with the observation that maximal effects of ABA on innate immune cells are observed at micromolar ABA concentrations (Bruzzone et al., 2007). Both R-(−) and S-(+) enantiomers ABA at high micromolar concentrations completely displaced binding of (R,S)-[$^3$H]-ABA to LANCL2-GST (Sturla et al., 2011). Instead, the metabolic effects of ABA on glucose transport *in vitro* and on glycemic control *in vivo* occur at nanomolar concentrations (Bruzzone et al., 2012; Magnone et al., 2015). This discrepancy suggested to perform a more in-depth investigation into the ABA binding affinity of human LANCL2. Indeed, docking results obtained by Lu and co-workers (2011) on a homology model of LANCL2, based on the crystal structure of LANCL1, highlighted several key contacts of LANCL2 with ABA.

With the aim of clarifying whether LANCL2 indeed has multiple ABA binding sites, possibly with different affinities for the hormone, we therefore performed new equilibrium binding studies with human recombinant LANCL2, exploring also the nanomolar range of ABA concentrations. In addition, orthogonal assays were performed using surface plasmon resonance (SPR) analysis to directly determine the binding of ABA to recombinant LANCL2. The observation of a hitherto undescribed high-affinity and saturable binding in the low nanomolar range prompted us to perform a new computational study, based on homology modeling of human LANCL2, followed by molecular docking of ABA. The hypothetical high-affinity ABA binding site suggested by the computational study was then confirmed by site-directed mutagenesis and both [$^3$H]-ABA saturation binding and SPR analysis on the mutated recombinant protein.

## 2. Materials and methods

### 2.1. Recombinant LANCL2 and site-directed mutants

Amino acid substitutions (R118I, R118I/R22I/K362I, and R118I/S41A/E46I) were generated using the QuickChange Lightning Site-Directed Mutagenesis kit (Agilent Technologies; Santa Clara, CA), following the manufacturer's instructions. Mutagenesis was performed directly on pGEX-6P-1 vector containing the full-length coding sequence of hLANCL2 (LANCL2-pGEX-6-P1) (Sturla et al., 2011). After mutagenesis, plasmids were used to transform *E. coli* XL10 (Agilent Technologies, Milan, Italy), then purified using Plasmid Mini Kit (Qiagen) and sequenced by TibMolbiol (Genova, Italy). The vectors containing the desired mutations were used to transform *E. coli* BL21 (DE3) (Agilent Technologies, Milan, Italy) and the colonies that produced the greatest amount of protein were used to express the mutant enzymes as glutathione *S*-transferase (GST)-fusion proteins, where GST was fused at the N-terminus of LANCL2.

Protein expression and purification were performed as described (Sturla et al., 2011), with some modifications detailed below. Wild-type and mutant LANCL2 were purified by affinity chromatography and the GST-tag was removed using PreScission Protease (GE Healthcare), by incubating the GSH-Sepharose-bound fusion protein for 16 h at 4 °C in Tris–HCl pH 7.5, 150 mM NaCl ("cleavage buffer"). Before being incubated with GSH-Sepharose, PreScission Protease was activated on ice, in the presence of 20 μM dithiothreitol (DTT) for 30 min. The final concentration of DTT during cleavage of the recombinant fusion protein was approximately 50 nM. The LANCL2-GST recombinant fusion protein was used for SPR analysis; the fusion protein was eluted from GSH-Sepharose–4 B by incubating the matrix at 25 °C for 15 min with 10 mM GSH in 50 mM Tris-HCl, pH 8. Recombinant proteins were concentrated using Amicon Ultra-15 centrifugal filter devices (Millipore, Milan, Italy) while continuously adding the cleavage buffer without DTT, to reduce the DTT concentration to less than 5 nM. Thus, the final protein solution was concentrated to a final concentration above 5 mg/ml in the same buffer used for binding experiments (150 mM NaCl, 50 mM Tris–HCl, pH 7.4, 1 mM EDTA). Protein concentrations were determined

according to Bradford (1976) using IgG as standard while protein purity was monitored by SDS–PAGE and gel filtration chromatography analysis using a Superose 12 10/300 GL column (GE Healthcare) in 50 mM Tris-HCl, 150 mM NaCl, pH 7.4.

To heat-denature wild-type LANCL2, the recombinant protein (0.1 mg/ml) was heated at 56 °C for 3.5 min and used as negative control for [$^3$H]-ABA saturation binding.

### 2.2. [$^3$H]-ABA binding

(R,S)-[$^3$H]-ABA saturation binding experiments were performed with the following recombinant LANCL2 proteins: wild-type LANCL2, three different mutagenized LANCL2 proteins, mutated at site 1 (R118I) or at sites 1 and 2 (R118I/R22I/K362I) or at sites 1 and 3 (R118I/S41A/E46I), and heat-denatured LANCL2 as control. Incubations were performed with 10 µg protein in 150 mM NaCl, 50 mM Tris–HCl pH 7.4, 1 mM EDTA (binding buffer) in a final volume of 100 µl in triplicate for 60 min at 25 °C with 0.05 µM (R,S)-[$^3$H]-ABA (20 Ci/mmol, Biotrend Radiochemicals, Köln, Germany), in the presence of increasing concentrations of unlabeled ABA (50 nM–5 mM) (Sigma–Aldrich). At the end of incubation, samples were filtered on 0.2 µm nitrocellulose membranes (Bio-Rad, Milan, Italy), the filters were washed with 3.5 ml ice-cold binding buffer and then dried, and the radioactivity was measured in 4.0 ml Ultima-Gold (Perkin Elmer, Italy) with a Packard β-counter. The specific (R,S)-[$^3$H]-ABA binding was calculated as the difference between total binding and non-specific binding, obtained with excess unlabeled (R,S)-ABA (5.0 mM). The maximal binding capacity (Bmax) and the dissociation constant ($K_D$) were calculated using the program Saturation Binding, specific binding only, in the GraphPad Prism 5.0 Software, San Diego, CA, USA. In this program the data are analysed by non-linear regression fit.

### 2.3. Surface plasmon resonance

Direct binding of unlabeled ABA to wild-type LANCL2-GST and LANCL2-R118I-GST was measured by surface plasmon resonance (SPR) on a Biacore T200 instrument (GE Healthcare) at 25° using a CM7 sensor chip (GE Healthcare). The covalent coupling of LANCL2-GST and LANCL2-R118I-GST on separate channels of the chip was accomplished through standard amine coupling and resulted in the immobilization of 24,860 and 24,390 resonance units (RUs) respectively. For both proteins, a surface without immobilized protein was used as a reference channel. All experiments were performed with a running buffer consisting of PBS with the addition of 0.05% Tween 20 (PBS-P) using a flow rate of 30 µl/min.

The evaluation of ABA binding to each protein was performed by injecting ABA dissolved in PBS-P in two different concentration ranges in separate experiments. The nanomolar concentration range consisted of ABA at 50 nM, 100 nM, 200 nM, 400 nM, and 600 nM and the micromolar range consisted of ABA at 1 µM, 2.5 µM, 5 µM, 10 µM, and 20 µM. ABA injections were done at a flow rate of 30 µl/min with a contact time of 8 s (s) and a dissociation time of 60 s. Bound ABA was removed by a subsequent regeneration step through the injection of 1 M NaCl for 30 s at 30 µl/min. The obtained sensorgrams were used for equilibrium state affinity analysis using the Biacore Evaluation software version 3.1 (GE Healthcare).

### 2.4. Ligand modeling

The chemical structure of ABA and related analogues were built, parameterized (Gasteiger-Hückel method) and energy minimized within Sybyl-X 1.0 using Tripos force field (Cichero et al., 2013a).

### 2.5. LANCL2 homology modeling

Since most of the residues characteristic of LANCL1 are conserved in LANCL2, the model we generated was developed starting from the X-ray structure of hLANCL1 (PDB code: 3E6U; resolution = 2.80 Å) (Zhang et al., 2009) obtained from the Protein Data Bank (Berman et al., 2000). The amino acid sequence of hLANCL2 (Q9NS86) was retrieved from the SWISSPROT database (Bairoch and Apweiler, 2000).

The alignment of the two enzyme sequences was made on the basis of the Blosum62 matrix (MOE software). The connecting loops were constructed by the loop search method implemented in MOE. This software developed the output files, including a series of ten receptor models, which were independently built using a Boltzmann-weighted randomized procedure (Levitt, 1992), taking into account a procedure concerning a proper handling of sequence insertions and deletions (Fechteler et al., 1995). The model endowed with the best packing quality function was selected for further energy minimization within the AMBER94 force field (Cornell et al., 1995). The energy minimization was carried out by the 1000 steps of steepest descent followed by conjugate gradient minimization until the rms gradient of the potential energy was less than 0.1 kcal $mol^{-1}$ $Å^{-1}$.

A thorough evaluation of the final chosen model was performed using Ramachandran plots, generated within MOE, and by exploring the energetic profile and the contact energy values of the hLANCL2 homology model we built. The derived information was compared with that calculated from the X-ray structure of the hLANCL1.

In addition, quality estimates for the modeled protein side-chain, evaluated by the rotamer energy profile, based on the methodology described by Dunbrack and Cohen (1997), as described in a previous study (Cichero et al., 2013a), displayed the absence of outliers.

### 2.6. Molecular docking studies

Molecular docking studies were performed considering four putative binding sites for (S)-2-cis, 4-trans ABA, the most abundant enantiomer in nature. In detail, we explored any suggested cavity proposed by the Site Finder module of MOE software, focusing our attention on the three best scored, the first one being retained as the most probable (site 1). The other two sites were also explored as second (site 2) or third putative binding sites (site 3).

The purpose of Site Finder is to calculate possible active sites in a receptor from the 3D atomic coordinates of the receptor. Such a calculation is useful for guiding site-directed mutagenesis experiments, in order to help determine potential sites for ligand binding docking calculations.

MOE's Site Finder falls into the category of geometric methods in the search of putative binding site, since no energy models are used. Instead, the relative positions and accessibility of the receptor atoms are considered, along with a rough classification of chemical type. The Site Finder methodology revolves around the development and matching with the protein of convex hulls, namely Alpha Spheres, featuring a different polarity profile. In brief, the method is as follows: (i) Identify regions of tight atomic packing, also on the surface of the protein. (ii) Filter out sites that are “too exposed” to solvent and retain all the others which are further classified based on their hydrophobic/hydrophilic properties. This is made by collecting a variable number of the aforementioned alpha spheres, which properly fit any putative site.

In addition, we also took into account the information described in the literature about a previously discussed LANCL2 homology model (Lu et al., 2011), where a putative ABA-binding site was reported (site 4).

Thus, the compounds were docked within the modeled hLANCL2 running four series of site-directed docking procedures, one for each putative binding site, by means of the LeadIT 2.1.8 software suite (www.biosolveit.com), including the FlexX scoring algorithm which is based on the calculation of the free binding energy by means of Gibbs-Helmholtz equation (Böhm, 1992,1994; Rarey et al., 1996). The software detects the binding site around the key residues as deciphered by MOE Site-finder, to set up a spherical search space for the docking

approach.

The standard setting for the docking strategy was followed, choosing the so-called Hybrid Approach (enthalpy and entropy criteria); the related scoring function evaluation is described in the literature (Bichmann et al., 2014). The derived docking poses were prioritized by the score values of the lowest energy pose of the compounds docked to the protein structure. All ligands were refined and rescored by assessment with the algorithm HYDE, included in the LeadIT 2.1.8 software. The HYDE module considers dehydration enthalpy and hydrogen bonding (Reulecke et al., 2008; Schneider et al., 2012).

Finally, the derived protein-ABA complex stability was successfully assessed using a short ~1 ps run of molecular dynamics (MD) at constant temperature, followed by an all-atom energy minimization (LowModeMD implemented in MOE software).

All calculations were carried out on a standard personal computer running under Windows XP.

## 3. Results

### 3.1. High-affinity ABA binding to human recombinant LANCL2

Human recombinant LANCL2 was expressed as an N-terminal fusion protein with the enzyme glutathione *S*-transferase (GST), but a significant modification to the previously described purification method (Sturla et al., 2011) was introduced. Here, LANCL2 was released from the LANCL2-GST fusion protein immobilized on glutathione-Sepharose–4B by incubation with PreScission Protease, pre-activated with DTT in a separate incubation. Thus, LANCL2 cleaved from GST was not exposed to the high DTT concentration required for activation of the PreScission Protease, described in the previously published protocol (Sturla et al., 2011). LANCL2 purity was checked by SDS-PAGE, which revealed a single band at approximately 50 kDa as expected (Supplementary information Fig. S1, A). LANCL2 and LANCL2-GST were both eluted from a gel filtration column as single symmetrical peaks confirming the purity of the proteins (Supplementary information Fig. S1, B). Saturable binding of (R,S)-[$^3$H]ABA to human purified LANCL2 was explored at ligand concentrations ranging from 50 nM to 50 μM ABA, with several concentrations tested in the nanomolar range (Fig. 2B). Wild-type, heat-denatured hLANCL2 was used as negative control. This protein showed no specific ABA binding (i.e. no displacement by excess unlabeled ABA – Fig. 2A, B).

Results obtained revealed a complex binding curve, with apparently two different plateaus (Fig. 2C). When the ligand binding affinity was calculated separately in the nanomolar and in the micromolar concentration range, two different binding constants could be calculated: a $K_D$ in the nanomolar range (0.14 μM ± 0.06 μM, Fig. 2B) and another one in the micromolar range (9.8 μM ± 0.3 μM, Fig. 2A), the latter one approximately ten times lower than the previously published $K_D$ (Sturla et al., 2011).

Several reasons may explain the discrepancy between the earlier and the present results: i) as mentioned, the purification procedure used here for recombinant LANCL2 avoids the high DTT concentrations previously employed and may have resulted in a better conservation of the native protein structure that contains 15 cysteine residues in its sequence; ii) ABA binding was explored here over a wider range of nanomolar concentrations (50, 75, 100, 200, 300 and 500 nM) compared to the previous study, where a single nanomolar value was explored (50 nM ABA). Indeed, if all experimental points in the nanomolar range, except for the value at 50 nM, were removed from Fig. 2C, the calculated $K_D$ of LANCL2 for ABA would be 10 μM.

Initial SPR experiments were performed with the cleaved LANCL2 protein; however, without a fusion partner, the protein was found to be very unstable and degraded rapidly on the sensor chip surface. All subsequent SPR experiments were therefore performed using the N-terminal GST fusion protein, both for the wild-type and the R118I mutant. The CM7 chip, used for immobilization, allowed higher immobilization levels compared to the affinity-based chips. As previous experiments had shown the presence of at least two different affinity ABA binding sites, a nanomolar and micromolar injection series were used to acquire two different steady state affinities for the wild-type LANCL2-GST. In the μM injection series (1, 2.5, 5, 10, and 20 μM) an affinity constant of 1.8 μM ± 0.8 μM (n = 3) was measured (Fig. 2E) while in the nanomolar injection series (50, 100, 200, 400 and 600 nM) the affinity constant was determined to be 2.6 nM ± 1.2 nM (n = 3) (Fig. 2D).

The high-affinity binding constant revealed by the equilibrium binding experiments on human LANCL2 prompted us to undertake a homology modeling study, to obtain a model of the protein for the *in silico* exploration of putative ABA-binding sites.

### 3.2. LANCL2 homology modeling

The multiple alignments described in the literature between LANCL1 and LANCL2 from human, monkey, rat, mouse, cattle and zebrafish reveal that all these proteins are characterized by conserved GxxG, SH3- and GSH-binding motifs (Lu et al., 2011). Based on this information, and following a computational procedure we previously applied to other case studies (Cichero et al., 2013a,b), we derived a human LANCL2 model, starting from the alignment of the LANCL2 FASTA sequence (Q9NS86) with that of the human LANCL1 X-ray structure (pdb code: 3E6U), as shown in Fig. 3. Reliability of the alignment was confirmed by the high value of the pair-wise percentage of residue identity (PPRI) calculated between the two proteins (PPRI = 58.6%).

The hLANCL2 model derived from this alignment was superimposed on the coordinates of human LANCL1 (Fig. 4A), used as template for the homology modeling calculations. It resulted in a root mean square deviation value (RMSD) of 0.734 Å calculated on the carbon atoms alignment with respect to the X-rays coordinates of the template.

The geometry and the related backbone conformation of the model were inspected by Ramachandran plot, which showed R256 as the only outlier of the model (see Supporting information S2) and gave a good validation of the computational protocol applied. In addition, the structural reliability of the model was also evaluated by comparing the energetic profile of the derived hLANCL2 with that of the hLANCL1 template. In general, high negative values and positive energy terms correspond to residues which are expected to be oriented toward a hydrophobic and a hydrophilic environment, respectively. Notably, the observed energetic profile of the model proved to be highly comparable with that of the reference LANCL1 protein (Fig. 4B).

In addition, quality estimates for the modeled protein side-chain were also evaluated by the rotamer energy profile, displaying absence of outliers (see Supporting information S3). Altogether, these data were interpreted as a general validation of the LANCL2 model and the exploration of the putative ABA binding sites was undertaken on this model.

### 3.3. Analysis of LANCL2 ABA-binding sites

In the absence of experimental data revealing the binding site of this protein, we deemed interesting to evaluate any possible and reasonable protein region which could be involved in the ABA binding process, through a specific computational approach based on homology modeling, docking and low molecular dynamics simulation studies (Cichero et al., 2013a). Accordingly, we started our work exploring the putative binding pockets as predicted by the Site Finder module of MOE software (see Materials and Methods), as we successfully did in previous case studies (Cichero et al., 2013b).

This software identified several possible ABA-binding sites: in particular, we focused our attention on the binding site with the highest score (henceforth called Site 1, Fig. 5a), on a second site with a similar

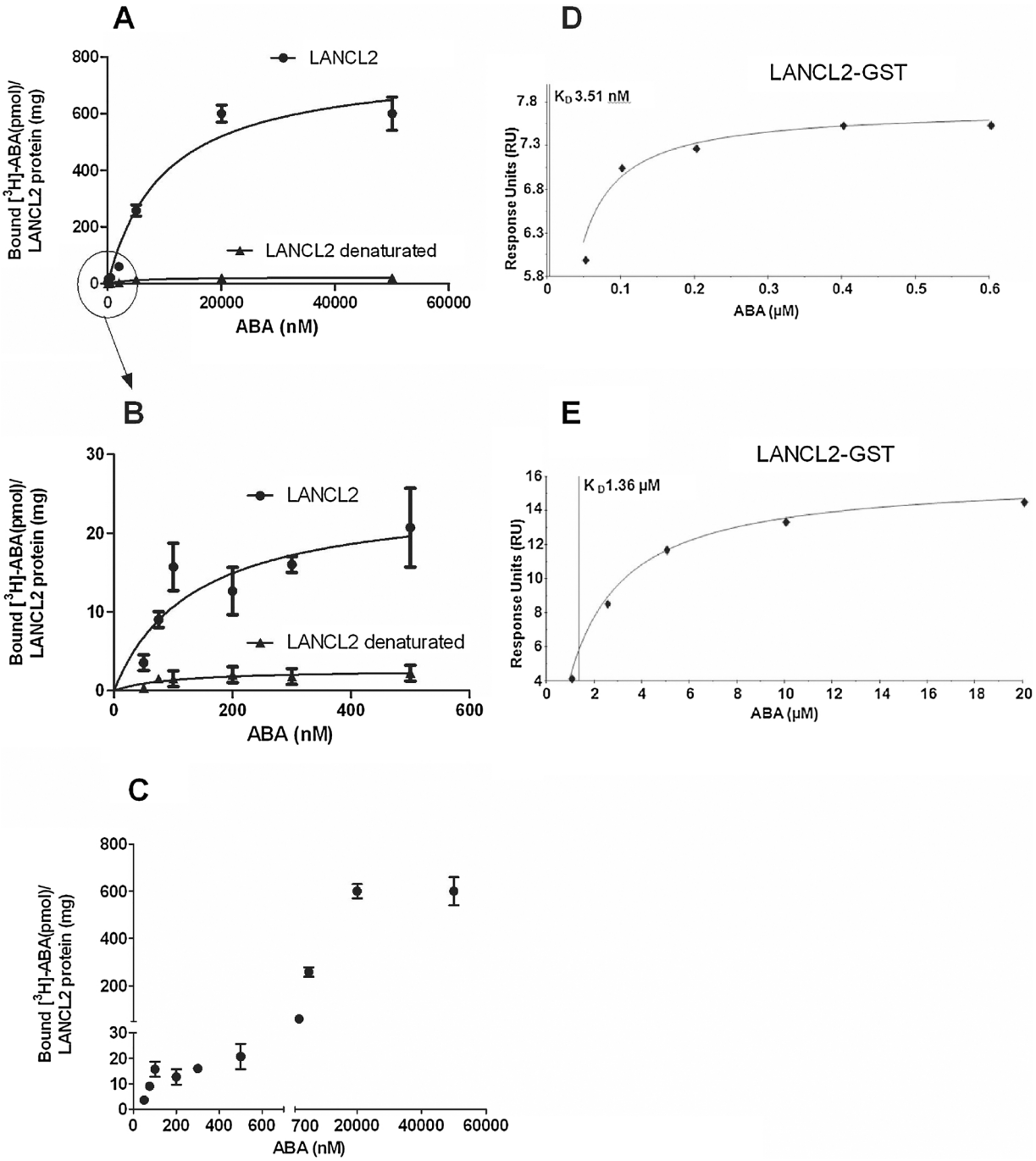


**Fig. 2.** Equilibrium binding of (R,S)-[$^3$H]-ABA and SPR assays on recombinant human LANCL2 reveals multiple binding sites. (**A**) Saturation binding experiments were performed as described in the Experimental Section. Human purified LANCL2 protein was incubated with 50 nM (R,S)-[$^3$H]-ABA in the presence of increasing concentrations of unlabeled ABA. The specific binding was analyzed in the micromolar range (A) and in the nanomolar concentration range (see inset, (**B**) by nonlinear regression, using the GraphPad Prism software. (**C**) representation of overall data points of specific binding to create a plot with a break in the axis indicating the shape of the curve, Results are the mean ± SD of 9 experiments. (**D**) SPR measurements of ABA binding to LANCL2-GST in a nM concentration range (0–600 nM). Steady-state $K_D$ values were estimated using the Biacore T200 evaluation software and reported as mean ± SD (n = 3). In this representative curve the $K_D$ is 3.51 nM and the chi-squared value is 0.30%. (**E**) SPR measurements of ABA binding to LANCL2-GST in a μM concentration range (0–20 μM). Steady-state $K_D$ values were estimated using the Biacore T200 evaluation software and reported as mean ± SD (n = 3). In this representative curve the $K_D$ is 1.36 μM and the chi-squared value is 0.17%.

score (henceforth called Site 2, Fig. 5b), and a third site with a lower score compared with Site 1 (henceforth called Site 3, Fig. 5c). We also took into account the literature data about a previous LANCL2 homology model (Lu et al., 2011), which suggested a possible ABA-binding site (henceforth called Site 4). A representation of putative ABA-binding sites which have been identified and explored is shown in Fig. 5. Interestingly, Site 1 is adjacent to the region proposed as Site 2, suggesting the possibility of mutual interference on their flexibility, through a related conformational change. Most residues of Site 1 fall into two helix domains (delimited by W106-R138 and R200-I214, respectively), and include L111, L114, R118, Q115 and Y205, Y209, T212 and E213.

The Q282-R297 helix region is involved in Site 2 through residues Q282, E283, T284, L285, T286, E287, in tandem with a pattern of amino acids belonging to three loop regions (R409-R413; R316-H322; K362-H368). Interestingly, a comparison performed between the

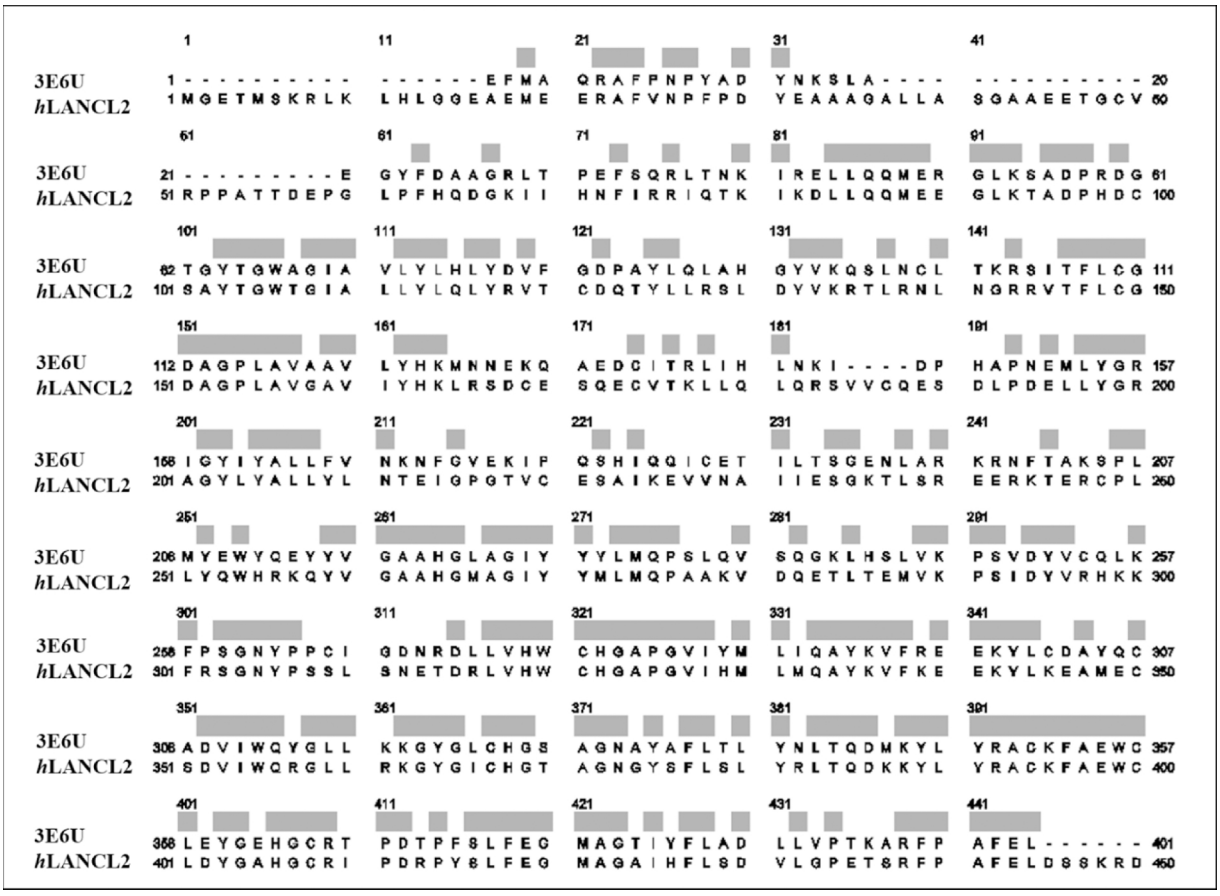


**Fig. 3.** Alignment of the *h*LANCL2 sequence on the *h*LANCL1X-ray structure (pdb code = 3E6U). Conserved residues are highlighted by grey bars.

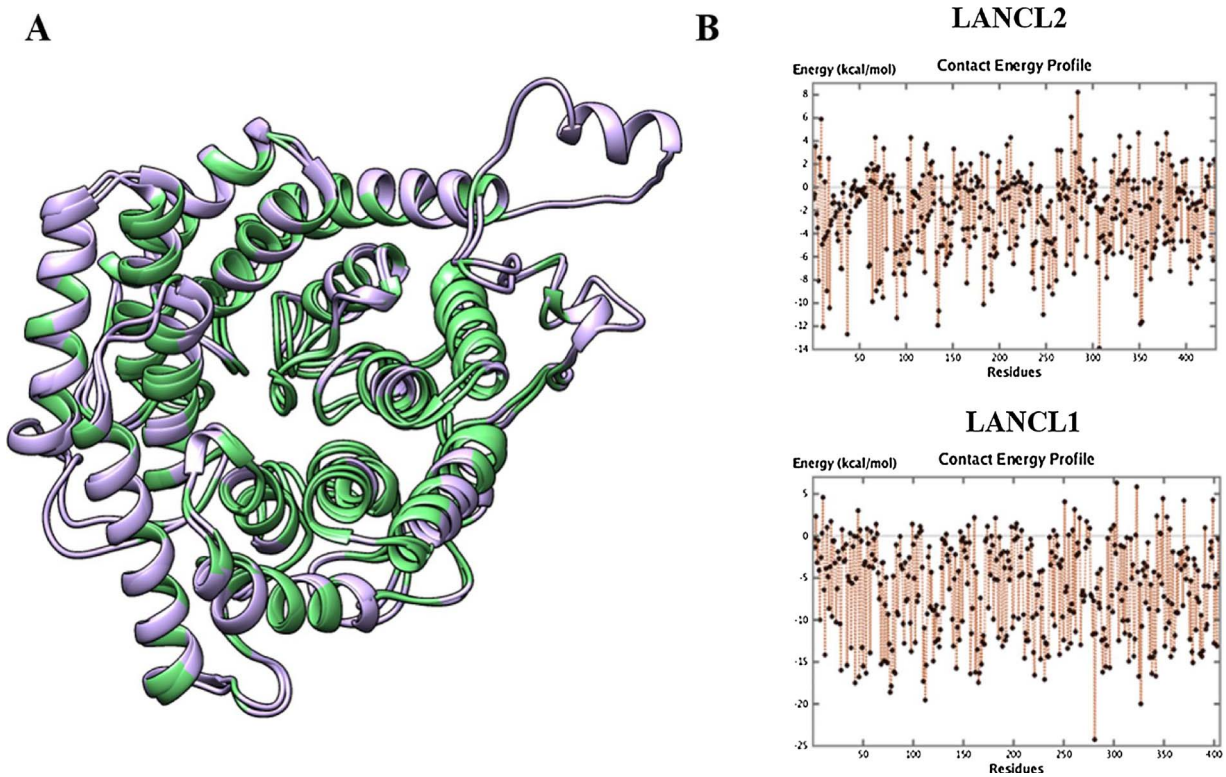


**Fig. 4.** Comparison between hLANCL2 and hLANCL1. (**A**) Superimposition of the hLANCL2 model derived from the sequence alignment with LANCL1 on the LANCL1 X-ray structure (3E6Uco-ordinates). The conserved regions are shown in light green (**B**) Contact energy profile of the hLANCL2 model compared with that of the hLANCL1 template. (For interpretation of the references to colour in this figure legend, the reader is referred to the web version of this article.)

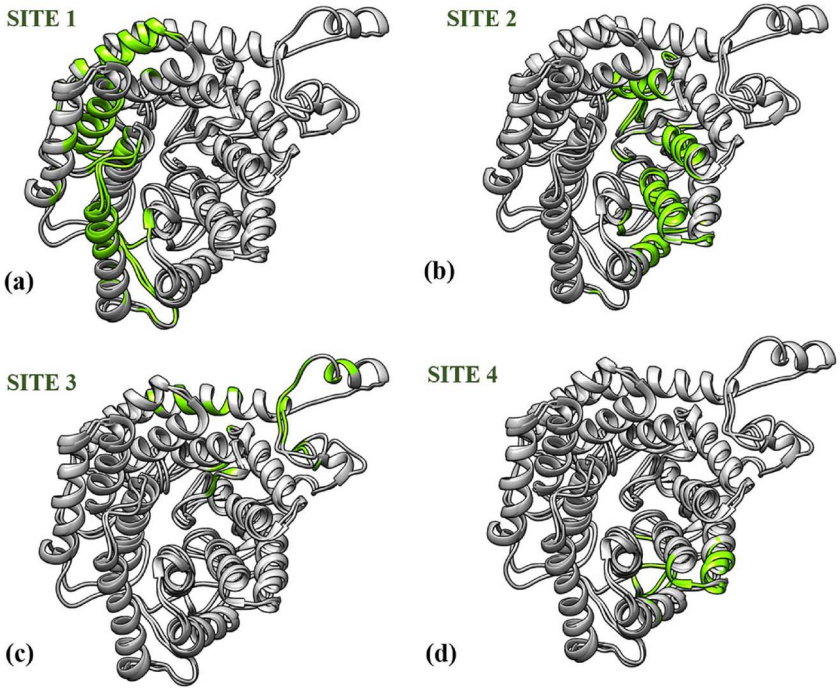


**Fig. 5.** A schematic representation of putative ABA-binding sites within the modeled hLANCL2, superimposed on the hLANCL1 structure (in grey). The regions involved in ABA-binding in the four sites are depicted in green.

residues belonging to Site 1 and to Site 2 and the corresponding cavities of hLANCL1, revealed an increase of the PPRI value in both cases (PPRI = 66.7% and 87.5%, respectively) for the two homologous proteins.

Compared with Site 1, Sites 3 and 4 are quite narrow crevices placed at the periphery of loop domains and characterized by the amino acids Y31, S41, E46, C394 and Y295, K299, K300, F301, respectively. Concerning Site 4, Lu et al. (2011) reported H−bonds between ABA and the K299 side-chain ε amino-group.

To identify the putative high-affinity binding site of ABA, molecular docking analyses were then performed on each site. The relevance of the obtained hLANCL2-ABA complexes was subsequently compared on the basis of SurFlex scoring functions and analyzed in terms of reasonable key contacts, after performing low molecular dynamics (MD) simulations.

### 3.4. ABA molecular docking studies

Based on an overall analysis of the docking calculations proposed here, we can infer that the binding poses shown for ABA are energetically quite comparable at site 1, slightly less at site 2, followed by site 3, while there is not a binding free energy advantage at site 4 (see Table 1). Thus, we took into consideration only the docking mode at sites 1, 2 and 3.

Preliminary docking results running on site 1 suggest a pattern of H−bond contacts involving the carbonyl oxygen of ABA and H426, while the hydroxyl group is engaged in one H−bond interaction with E213. Notably, the refined docking pose obtained with low MD confirmed the previously cited contacts and also highlighted a further electrostatic bond between the carboxyl group of ABA and the R118 side-chain (Fig. 6A).

According to our docking calculations, the most probable positioning of ABA within site 2 is related to the formation of polar contacts between the carboxylic acid group and the R22 and R316 side-chains (not shown), while the hydroxyl function is involved in H−bonds with K362. All these interactions were verified by low MD that in addition pointed out the relevance of a further H−bond involving the carbonyl oxygen atom and the Y103 side-chain (Fig. 6B).

Finally, the most probable driving force underlying the ABA docking mode within site 3 is represented by H−bonds between the carboxylic group and S41, and between the hydroxyl moiety and the E46 side-chain (Fig. 6C). In the case of site 3, less effective electrostatic contacts contribute to the ligand stabilization compared with sites 1 and 2, in agreement with the values of binding affinity energies shown in Table 1.

Based on these results, sites 1, 2 and 3 emerged as possible ABA-binding sites in hLANCL2, with site 1 being the most probable, possibly representing the high-affinity binding site for ABA. Thus, we decided to perform a site-directed mutagenesis of site 1, with and without the concomitant mutation in either one of the other sites (site 2 or site 3), and to repeat the binding experiments on the mutated proteins.

**Table 1**
Binding affinity values obtained by molecular docking studies of ABA within site 1, 2, 3 and 4.

| Enzyme-Ligand Complex (LeadIT) | Binding Affinity Energy ΔG (kJ/mol) |
|---|---|
| Site 1-ABA | −24.0 |
| Site 2- ABA | −20.0 |
| Site 3- ABA | −9.0 |
| Site 4- ABA | −2.0 |

### 3.5. ABA binding to mutagenized hLANCL2

Single or multiple mutants of human LANCL2 were generated by site-directed mutagenesis: i) the single mutant R118I, with a mutated site 1; ii) the triple mutant R118I/R22I/K362I, with a mutated site 1 and a mutated site 2, and iii) the triple mutant R118I/S41A/E46I, with a mutated site 1 and a mutated site 3. The amino acids to be mutated were chosen among those involved in contacts with the ligand, preferring the ones establishing polar interactions with ABA. The substituting amino acid was preferentially Isoleucine, to eliminate the polarity of the original residue, while at the same time providing a bulky, space-filling substitute; Serine 41 was substituted with the

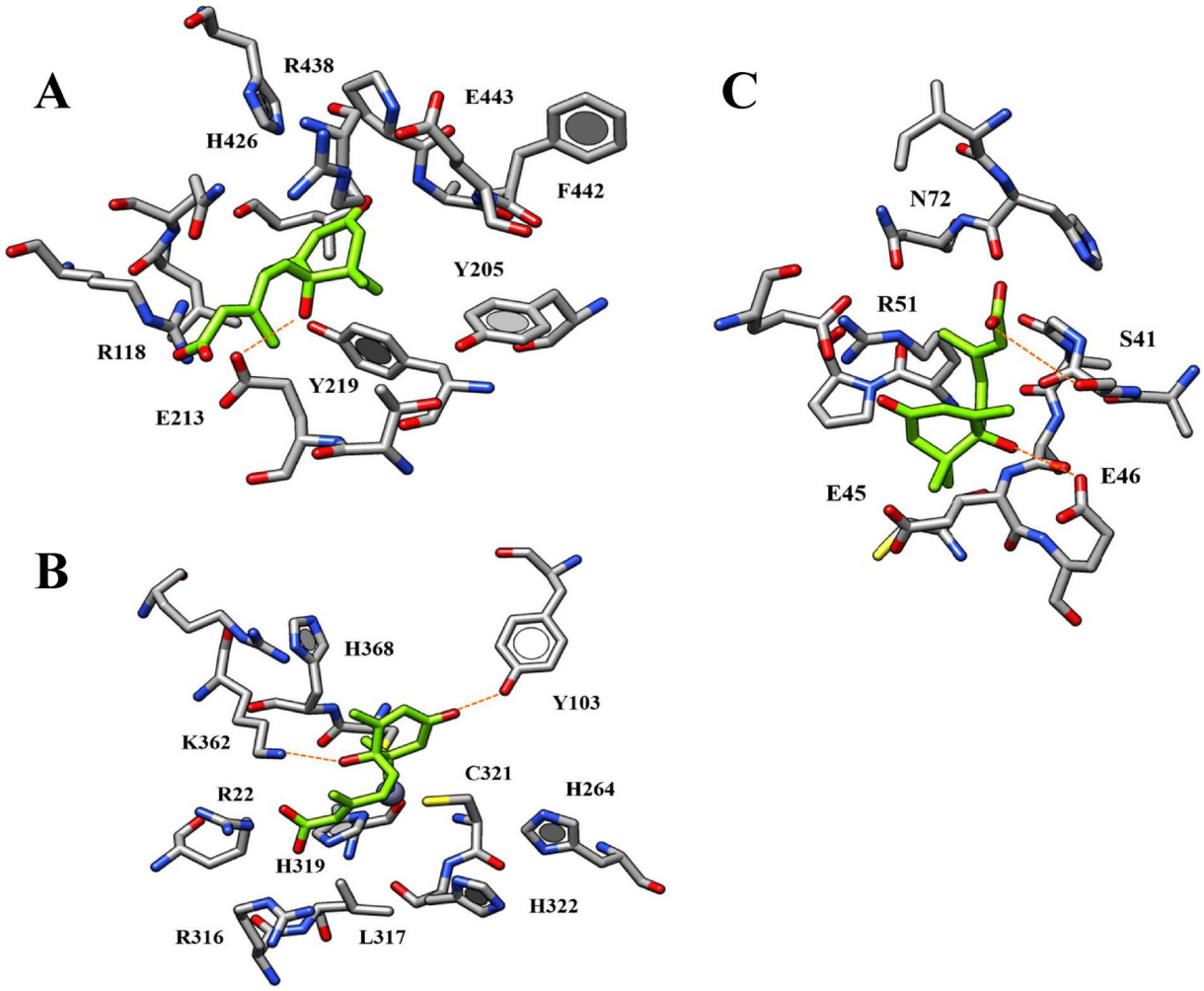


**Fig. 6.** Low MD-refined docking mode of ABA within Site 1 (**A**), Site 2 (**B**), Site 3 (**C**) of hLANCL2. For the sake of clarity, only the most important residues are indicated. H−bonds are shown by orange dot-line. (For interpretation of the references to colour in this figure legend, the reader is referred to the web version of this article.)

similarly small hydrophobic Alanine.

Binding of (R,S)-[$^3$H]ABA to the different recombinant proteins was compared with binding to wild-type, non-mutagenized, hLANCL2. Wild-type, heat-denatured hLANCL2 was used as negative control.

Upon substitution of R118 with an Ile in site 1 the high-affinity ABA-binding site was lost (Fig. 7A), but saturation did still occur at high (tens of micromolar) ABA concentrations (Fig. 7B), indicating presence of other(s), low-affinity binding site(s), unaffected by the R118I substitution.

SPR analysis performed using the same two injection series as those used for the wild-type protein, indeed confirmed this, as only the μM concentration range allowed the determination of an affinity constant (1.04 μM ± 0.7 (n = 2)) (Fig. 7C). Conversely, low-affinity ABA binding was significantly reduced when the mutations were introduced either in site 2 (R22I and K362I) or in site 3 (S41A and E46I, Fig. 7B). Both triple mutations greatly reduced the calculated Bmax value compared with the wild-type protein, while the single mutation in site 1 did not. Bmax values were 1205, 1946, 240 and 467 pmol/mg for wtLANCL2, LANCL2 mutated in site 1 only, LANCL2 mutated in sites 1 and 2, and LANCL2 mutated in sites 1 and 3, respectively.

## 4. Discussion

Altogether, results reported here reveal the presence of a high-affinity ABA-binding site (with a $K_D$ in the nanomolar range) and two low affinity ABA-binding sites ($K_D$ in the micromolar range) on human recombinant LANCL2. These results were obtained on two different human recombinant LANCL2 proteins (the protein fused with GST and the cleaved, purified protein) and with two different equilibrium binding techniques ([$^3$H]-ABA binding and SPR).

LANCL2-GST has a low-affinity $K_D$ for ABA of 1.8 μM ± 0.8 μM as detected by SPR, a value comparable to the one previously obtained by [$^3$H]-ABA equilibrium binding (Sturla et al., 2011). LANCL2 cleaved from GST has a tendency to precipitate, particularly at high protein and DTT concentrations. In order to confirm the presence of the high affinity ABA binding site on LANCL2 in the absence of GST, [$^3$H]-ABA binding was nonetheless explored on the protein, cleaved under low-DTT concentrations. Indeed, the low affinity $K_D$ value reported here (10 μM) is ten times lower than the previously reported value for cleaved LANCL2 (Sturla et al., 2011), suggesting that removal of DTT improved the protein's binding performance; in addition, presence of a high-affinity ABA binding site involving R118 was also demonstrated. While SPR could not be performed on the cleaved LANCL2, due to precipitation of the protein on the chip surface, SPR performed on LANCL2-GST confirmed presence of a high-affinity binding site for ABA (with a $K_D$ of 2.6 nM ± 1.2 nM) and also that high-affinity ABA binding is lost upon mutation of R118.

Native human LANCL2 is N-myristoylated and located at the inner side of the plasma membrane, where it interacts with a G-protein (Fresia et al., 2016). Thus, it is not surprising that recombinant LANCL2, cleaved from GST, is less stable in solution compared with the fusion protein. However, circular dichroism analysis of LANCL2 cleaved

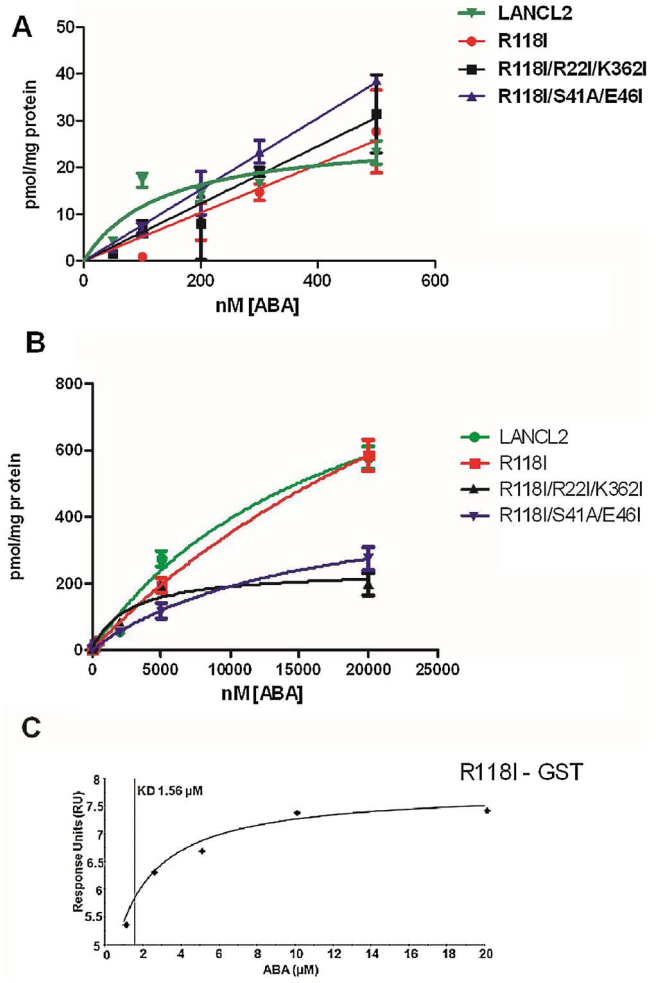


**Fig. 7.** Equilibrium binding of (R,S)-[$^3$H]-ABA to mutagenized hLANCL2 identifies site 1 as the high-affinity ABA-binding site. Mutagenesis, protein expression and purification were performed as described in the Experimental Section. Binding of (R,S)-[$^3$H]-ABA to the different recombinant proteins was compared with binding to wild-type LANCL2 (green) in the nanomolar (**A**) and in the micromolar (**B**) concentration range. The specific [$^3$H]-ABA binding was calculated as the difference between total binding and nonspecific binding (in the presence of 5 mM unlabeled ABA) using GraphPad Prism software. Results are the mean ± SD of 3 different experiments. (**C**) SPR measurements of ABA binding to mutant LANCL2-GST in a µM concentration range (0–20 µM). Steady-state $K_D$ values were estimated using the Biacore T200 evaluation software and reported as mean ± SD (n = 2). In this representative curve the $K_D$ is 1.56 µM and the chi-squared value is 0.75%. (For interpretation of the references to colour in this figure legend, the reader is referred to the web version of this article.)

from the GST fusion protein performed in parallel with LANCL1, similarly cleaved from GST, yielded similar spectra of the two proteins characterized by the presence of two peaks at about 209 and 222 nm, typical of α-helix conformation (not shown). The fact that two different equilibrium binding techniques, performed on the fused and the cleaved protein, both revealed the presence of a high-affinity ABA binding site with a nanomolar $K_D$, which is lost upon mutation of R118, strengthens the conclusion that indeed a high-affinity binding site for ABA is present on LANCL2.

The nanomolar and micromolar affinity constants detected in this study on human recombinant LANCL2 are in the range of the ABA concentrations endowed with metabolic and inflammation-related effects, respectively, observed both *in vitro* and *in vivo* (Bruzzone et al., 2007, 2008, 2012; Magnone et al., 2015). Indeed, LANCL2 has been proposed as a target for anti-diabetic and anti-inflammatory interventions (Lu et al., 2014; Lievens et al., 2017). If the metabolic and inflammation-related effects of ABA were mediated by its occupancy of the high- or the low-affinity binding sites, respectively, the development of site-specific agonists/antagonists could be envisaged, to selectively affect one or the other of the functional effects of ABA.

Analysis with the GraphPad Software of the binding curve of [$^3$H]-ABA to LANCL2, over a concentration range spanning from low nanomolar to millimolar values (Fig. 2C), reveals a Hill coefficient of 1.9 ± 0.3. Similar Hill coefficient values, ranging from 1.4 ± 0.3 to 2.0 ± 0.5 were determined from the SPR data. All these values consistently suggest multiple binding sites with positive cooperativity. Identification of the molecular mechanisms underlying cooperativity will require a high resolution crystal structure of the protein; accordingly the physiological significance of this apparent cooperative effect between ABA-binding sites on LANCL2 is now open to investigation. Another issue requiring further studies is the specificity of the binding sites for the naturally occurring enantiomers of 2-cis, 4-trans ABA, (R)-ABA and (S)-ABA. Both enantiomers are active on animal cells (Bruzzone et al., 2007; Bruzzone et al., 2008) and each can displace binding of (R,S)-[$^3$H]-ABA from human recombinant LANCL2 at a concentration in the micromolar range (Sturla et al., 2011); from these observations, it can be hypothesized that both enantiomers can interact with the high and low-affinity binding sites, although confirmatory evidence needs to be obtained.

Identification of a high-affinity ABA binding site on hLANCL2 will pave the way to the design of high-affinity, site-specific ABA agonists/antagonists, which will help to understand the role of this binding site in ABA/LANCL2 signaling and function and in the molecular pathogenesis of metabolic and inflammation-related diseases (De Flora et al., 2014; Lievens et al., 2017; Zocchi et al., 2017). Moreover, identification of R118 as a critical amino acid residue in the high affinity binding site suggests to investigate presence of genetic polymorphisms at this site, which could be responsible for individual low-responsiveness to endogenous ABA, leading to an impairment of glucose tolerance.

## Competing financial interests

The authors declare no competing financial interests.

## Acknowledgments

PF and EC would like to thank Mr. V. Ruocco for the informatic support to calculations and Dr. A. Civino for his kind assistance. LI, HdJ and CS are grateful to Dr. M. Maggi for useful discussion and help with data elaboration. LS is grateful to Dr. Cristina D'Arrigo for useful discussion on circular dichroism analysis.

This work was financially supported by the University of Genova and by MIUR (grant #RBFR1299K0_002 to CF; grant #2010MCLBCZ_004 to EZ).

## Appendix A. Supplementary data

Supplementary data associated with this article can be found, in the online version, at https://doi.org/10.1016/j.biocel.2018.02.003.

## References

Böhm, H.J., 1992. The computer program LUDI: a new method for the de novo design of enzyme inhibitors. J. Comput.-Aided Mol. Des. 6, 61–78.

Böhm, H.J., 1994. The development of a simple empirical scoring function to estimate the binding constant for a protein?ligand complex of known three-dimensional structure. J. Comput. -Aided Mol. Des. 8, 243–256.

Bairoch, A., Apweiler, R., 2000. The SWISS-PROT protein sequence database and its supplement TrEMBL in 2000. Nucleic Acids Res. 28, 45–48.

Bauer, H., Mayer, H., Marchler-Bauer, A., Salzer, U., Prohaska, R., 2000. Characterization of p40/GPR69A as a peripheral membrane protein related to the lantibiotic synthetase component C. Biochem. Biophys. Res. Commun. 275, 69–74.

Berman, H.M., Westbrook, J., Feng, Z., Gilliland, G., Beth, T.N., Weissig, H., Shindyalov, I.N., Bourne, P.E., 2000. The protein data bank. Nucleic Acids Res. 28, 235–242.

Bichmann, L., Wang, W.T., Fischer, W.B., 2014. Docking assay of small molecule antivirals to p7 of HCV. Comput. Biol. Chem. 53, 308–317.

Bodrato, N., Franco, L., Fresia, C., Guida, L., Usai, C., Salis, A., Moreschi, I., Ferraris, C., Verderio, C., Basile, G., Bruzzone, S., Scarfì, S., De Flora, A., Zocchi, E., 2009. Abscisic acid activates the murine microglial cell line N9 through the second messenger cyclic ADP-ribose. J. Biol. Chem. 284, 14777–14787.

Bradford, M.M., 1976. Rapid and sensitive method for the quantitation of microgram quantities of protein utilizing the principle of protein-dye binding. Anal. Biochem. 72, 248–254.

Bruzzone, S., Moreschi, I., Usai, C., Guida, L., Damonte, G., Salis, A., Scarfì, S., Millo, E., De Flora, A., Zocchi, E., 2007. Abscisic acid is an endogenous cytokine in human granulocytes with cyclic ADP-ribose as second messenger. Proc. Natl. Acad. Sci. U.S.A. 104, 5759–5764.

Bruzzone, S., Bodrato, N., Usai, C., Guida, L., Moreschi, I., Nano, R., Antonioli, B., Fruscione, F., Magnone, M., Scarfì, S., De Flora, A., Zocchi, E., 2008. Abscisic acid is an endogenous stimulator of insulin release from human pancreatic islets with cyclic ADP-ribose as second messenger. J. Biol. Chem. 283, 32188–32197.

Bruzzone, S., Ameri, P., Briatore, L., Mannino, E., Basile, G., Andraghetti, G., Grozio, A., Magnone, M., Guida, L., Scarfì, S., Salis, A., Damonte, G., Sturla, L., Nencioni, A., Fenoglio, D., Fiory, F., Miele, C., Beguinot, F., Ruvolo, V., Bormioli, M., Colombo, G., Maggi, D., Murialdo, G., Cordera, R., De Flora, A., Zocchi, E., 2012. The plant hormone abscisic acid increases in human plasma after hyperglycemia and stimulates glucose consumption by adipocytes and myoblasts. FASEB J. 26, 1251–1260.

Cichero, E., D'Ursi, P., Moscatelli, M., Bruno, O., Orro, A., Rotolo, C., Milanesi, L., Fossa, P., 2013a. Homology modeling, docking studies and molecular dynamic simulations using graphical processing unit architecture to probe the type-11 phosphodiesterase catalytic site: a computational approach for the rational design of selective inhibitors. Chem. Biol. Drug Des. 82, 718–731.

Cichero, E., Espinoza, S., Gainetdinov, R.R., Brasili, L., Fossa, P., 2013b. Insights into the structure and pharmacology of the human trace amine-associated receptor 1 (hTAAR1): homology modelling and docking studies. Chem. Biol. Drug Des. 81, 509–516.

Cornell, W.D.C.P., Bayly, C.I., Gould, I.R., Merz, K.M., Ferguson, D.M., Spellmeyer, D.C., Fox, T., Caldwell, J.W., Kollman, P.A.J., 1995. A second generation force field for the simulation of proteins, nucleic acids and organic molecules. J. Am. Chem. Soc. 117, 5179–5196.

De Flora, A., Bruzzone, S., Guida, L., Sturla, L., Magnone, M., Fresia, C., Vigliarolo, T., Mannino, E., Sociali, G., Zocchi, E., 2014. Toward a medicine-oriented use of the human hormone/nutritional supplement Abscisic Acid. Messenger 3, 86–97.

Dunbrack, R.L., Cohen, F.E., 1997. Bayesian statistical analysis of protein side chain rotamer preferences. Protein Sci. 6, 1661–1681.

Fechteler, T., Dengler, U., Schomberg, D., 1995. Prediction of protein three-dimensional structures in insertion and deletion regions: a procedure for searching data bases of representative protein fragments using geometric scoring criteria. J. Mol. Biol. 253, 114–131.

Fresia, C., Vigliarolo, T., Guida, L., Booz, V., Bruzzone, S., Sturla, L., Di Bona, M., Pesce, M., Usai, C., De Flora, A., Zocchi, E., 2016. G-protein coupling and nuclear translocation of the human abscisic acid receptor LANCL2. Sci. Rep. 6, 26658.

He, C., Zeng, M., Dutta, D., Koh, T.H., Chen, J., van der Donk, W.A., 2017. LanCL proteins are not involved in lanthionine synthesis in mammals. Sci. Rep. 7, 40980.

Landlinger, C., Salzer, U., Prohaska, R., 2006. Myristoylation of human LanC-like protein 2 (LANCL2) is essential for the interaction with the plasma membrane and the increase in cellular sensitivity to adriamycin. Biochim. Biophys. Acta 1759–1767 1758s.

Levitt, M., 1992. Accurate modeling of protein conformation by automatic segment matching. J. Mol. Biol. 226, 507–533.

Lievens, L., Pollier, J., Goossens, A., Beyaert, R., Staal, J., 2017. Abscisic acid as pathogen effector and immune regulator. Front. Plant Sci. 8, 587.

Lin, B.L., Wang, H.J., Wang, J.S., Zaharia, L.I., Abrams, S.R., 2005. Abscisic acid regulation of heterophylly in Marsilea quadrifolia L.: effects of R-(−) and S-(+) isomers. J. Exp. Bot. 56, 2935–2948.

Lu, P., Bevan, D.R., Lewis, S.N., Hontecillas, R., Bassaganya-Riera, J., 2011. Molecular modeling of lanthionine synthetase component C-like protein 2: a potential target for the discovery of novel type 2 diabetes prophylactics and therapeutics. J. Mol. Model. 17, 543–553.

Lu, P., Hontecillas, R., Philipson, C.W., Bassaganya-Riera, J., 2014. Lanthionine synthetase component C-like protein 2: a new drug target for inflammatory diseases and diabetes. Curr. Drug Targets 15, 565–572.

Magnone, M., Bruzzone, S., Guida, L., Damonte, G., Millo, E., Scarfì, S., Usai, C., Palombo, D., De Flora, A., Zocchi, E., 2009. Abscisic acid released by human monocytes activates monocytes and vascular smooth muscle cells responses involved in atherogenesis. J. Biol. Chem. 284, 17808–17818.

Magnone, M., Ameri, P., Salis, A., Andraghetti, G., Emionite, L., Murialdo, G., De Flora, A., Zocchi, E., 2015. Microgram amounts of abscisic acid in fruit extracts improve glucose tolerance and reduce insulinemia in rats and in humans. FASEB J. 29, 4783–4793.

Mayer, H., Breuss, J., Ziegler, S., Prohaska, R., 1998. Molecular characterization and tissue-specific expression of a murine putative G-protein-coupled receptor. Biochim. Biophys. Acta 1399, 51–56.

Mayer, H., Pongratz, M., Prohaska, R., 2001. Molecular cloning, characterization, and tissue-specific expression of human LANCL2, a novel member of the LanC-like protein family. DNA Seq. 12, 161–166.

Nambara, E., Marion-Poll, A., 2005. Abscisic acid biosynthesis and catabolism. Annu. Rev. Plant Biol. 56, 165–185.

Rarey, M., Kramer, B., Lengauer, T., Klebe, G., 1996. A fast flexible docking method using an incremental construction algorithm. J. Mol. Biol. 261, 470–489.

Reulecke, I., Lange, G., Albrecht, J., Klein, R., Rarey, M., 2008. Towards an integrated description of hydrogen bonding and dehydration: decreasing false positives in virtual screening with the HYDE scoring function. Chem. Med. Chem. 3, 885–897.

Schneider, N., Hindle, S., Lange, G., Klein, R., Albrecht, J., Briem, H., Beyer, K., Claußen, H., Gastreich, M., Lemmen, C., Rarey, M., 2012. Substantial improvements in large-scale redocking and screening using the novel HYDE scoring function. J. Comput.-Aided Mol. Des. 26, 701–723.

Sturla, L., Fresia, C., Guida, L., Bruzzone, S., Scarfì, S., Usai, C., Fruscione, F., Magnone, M., Millo, E., Basile, G., Grozio, A., Jacchetti, E., Allegretti, M., De Flora, A., Zocchi, E., 2009. LANCL2 is necessary for abscisic acid binding and signaling in human granulocytes and in rat insulinoma cells. J. Biol. Chem. 284, 28045–28057.

Sturla, L., Fresia, C., Guida, L., Grozio, A., Vigliarolo, T., Mannino, E., Millo, E., Bagnasco, L., Bruzzone, S., De Flora, A., Zocchi, E., 2011. Binding of abscisic acid to human LANCL2. Biochem. Biophys. Res. Commun. 415, 390–395.

Zeng, M., van der Donk, W.A., Chen, J., 2014. Lanthionine synthetase C-like protein 2 (LanCL2) is a novel regulator of Akt. Mol. Biol. Cell 25, 3954–3961.

Zhang, W., Wang, L., Liu, Y., Xu, J., Zhu, G., Cang, H., Li, X., Bartlam, M., Hensley, K., Li, G., Rao, Z., Zhang, X.C., 2009. Structure of human lanthionine synthetase C-like protein 1 and its interaction with Eps8 and glutathione. Genes Dev. 23, 1387–1392.

Zocchi, E., Hontecillas, R., Leber, A., Einerhand, A., Carbo, A., Bruzzone, S., Tubau-Juni, N., Philipson, N., Zoccoli-Rodriguez, V., Sturla, L., Bassaganya-Riera, J., 2017. Abscisic acid: a novel nutraceutical for glycemic control. Front. Nutr. 4, 24.